



Purification of silk nanoparticles: impact of centrifugation and tangential flow filtration on critical quality attributes

Manuel Fischer^a , Annika Kahlenberg^a, Simone Berger^a , Frank Steiniger^b, Daniela Wissenbach^c, F. Philipp Seib^{a,d} 

^a Friedrich Schiller University Jena, Institute of Pharmacy, Department of Pharmaceutical Technology and Biopharmaceutics, Lessingstr. 8, 07743 Jena, Germany

^b Jena University Hospital, Center for Electron Microscopy, Friedrich Schiller University, Ziegelmühlenweg 1, 07743 Jena, Germany

^c Jena University Hospital, Institute for Forensic Medicine, Friedrich Schiller University Jena 07747 Jena, Germany

^d Fraunhofer Institute for Molecular Biology and Applied Ecology, Branch Bioresources, Ohlebergweg 12, 35392 Giessen, Germany

ARTICLE INFO

Keywords:
Nanomedicine
Purification
Bombyx mori
Silk

ABSTRACT

Silk has emerged as a promising biomaterial for formulating protein-based nanocarriers for use as drug delivery systems. Silk nanoparticles can be manufactured using several different methods, including nanoprecipitation through organic desolvation using isopropanol as an antisolvent. The translation of silk nanoparticle manufacture from the bench to the industrial scale requires deeper insights into the manufacturing process, especially nanoparticle purification. Here, we compare the impact of tangential flow filtration (TFF) with widely used centrifugation methods for silk nanoparticle purification. Silk nanoparticles were manufactured using a well-studied semi-batch nanoprecipitation process. We demonstrate that silk nanoparticle purification significantly changed the physicochemical properties, particularly the yield. The silk nanoparticles showed major differences in *in vitro* cytotoxicity, depending on the purification method used. TFF purification revealed that a change in permeate volume during purification was a key parameter, as low cytotoxicity was correlated with an increase in the diavolume. Overall, TFF emerges as a purification method with high potential for scale-up and faster silk nanoparticle purification.

1. Introduction

The critical quality attributes of nanoparticles, including their physicochemical properties, are important factors that determine the success of scaling up nanomedicine production from the bench to the manufacturing sector. (Taha et al., 2020) Similarly, the physicochemical properties of nanoparticles also regulate many other factors, such as drug loading, (Liu et al., 2020) long-term stability and *in vivo* performance. (Xu et al., 2023) In general, drug carriers sized between 100 and 200 nm with hydrophilic and negatively charged shells are well-suited for drug delivery. (Matthew & Seib, 2025).

One promising drug delivery material with interesting properties in terms of biodegradability, biocompatibility and mechanical strength is *Bombyx mori* (*B. mori*) silk. (Tran et al., 2023; Holland et al., 2019) Silk is amenable to different nanoparticle fabrication methods, including single or double emulsification, (Baimark et al., 2010) nanoprecipitation, (Matthew et al., 2020) and salting out. (Matthew & Seib, 2025) During the fabrication process, the drug is typically encapsulated in the nanoparticles, followed by a purification process to remove additives,

surfactants, and/or unencapsulated drug molecules. (Shah et al., 2020).

The most common method for silk nanoparticle manufacture is nanoprecipitation using an organic solvent, which must be removed before the nanoparticles can be used. (Matthew et al., 2020; Wongpiyo-chit et al., 2019) Next, centrifugal force is used to separate the final nanoparticle products from undesired materials. (Tehrani et al., 2025) Another approach is to use diafiltrating centrifugal devices, which separate nanoparticles from raw materials by applying a centrifugal force through filters with a defined weight cut-off (MWCO). (Dalwadi et al., 2005; Mihaila et al., 2011) Although these separation methods are simple and convenient, the gravitational forces generated during centrifugation can alter nanoparticle properties by causing caking and dense pellet packing, which then require laborious redispersion (Dalwadi & Sunderland, 2008, 2007) Redispersion by ultrasonication can lead to further inconsistencies in nanoparticle characteristics, resulting in batch-to-batch variations. (Mülhopt et al., 2018).

To overcome these limitations, alternative purification strategies must be explored. Among these, tangential flow filtration (TFF) is particularly promising. TFF is already widely used for the purification of

E-mail address: philipp.seib@uni-jena.de (F.P. Seib).

<https://doi.org/10.1016/j.ijpharm.2025.126436>

Received 26 September 2025; Received in revised form 21 November 2025; Accepted 24 November 2025

Available online 29 November 2025

0378-5173/© 2025 The Authors. Published by Elsevier B.V. This is an open access article under the CC BY license (<http://creativecommons.org/licenses/by/4.0/>).

biomolecules (e.g. proteins), food and beverages, as well as water filtration. As the name suggests, TFF purification is achieved by flowing a fluid tangentially to a filter, enabling dynamic purification. This contrasts with conventional dead-end filtration methods, where the fluid flows perpendicularly to the membrane, potentially resulting in membrane caking and subsequent decreases in the overall permeate flux across the membrane. With TFF, the dispersions of interest can be retained while efficiently removing waste products. One advantage of TFF is the constant concentration gradient, as this enables the removal of excess media while also reconcentrating solutes. (Musumeci et al., 2018) TFF is scalable and enables size-selective separation while preserving nanoparticle integrity (Dizon-Maspat et al., 2012; Gagnon, 2012; Musumeci et al., 2018).

Despite recent advances in TFF protocols and their use (Tomeh et al., 2022), no study has yet analysed the impact of TFF on the characteristics of silk nanoparticles purified with this method. The purpose of the present study was to compare the impact of TFF processing versus

conventional centrifugation purification on silk nanoparticle quality attributes. Here, the TFF parameters, namely flow rate and trans-membrane pressure, were kept constant. These constant hydrodynamic conditions were used to assess silk nanoparticle purification, particularly solvent removal, thereby addressing a key knowledge gap and advancing the biomedical use of silk Fig. 1.

2. Materials and methods

Unless otherwise specified, all experiments were conducted at 18–25 °C. Chemicals were obtained from commercial suppliers and used without further purification. Anhydrous sodium carbonate was purchased from Merck KGaA (Darmstadt, Germany) and lithium bromide (99 % purity) was obtained from Thermo Fisher Scientific (Waltham, MA, USA). Isopropanol (≥ 99.5 %, for synthesis) was purchased from Carl Roth (Karlsruhe, Germany).

Regeneration of Silk. Silk fibroin was extracted from *B. mori*

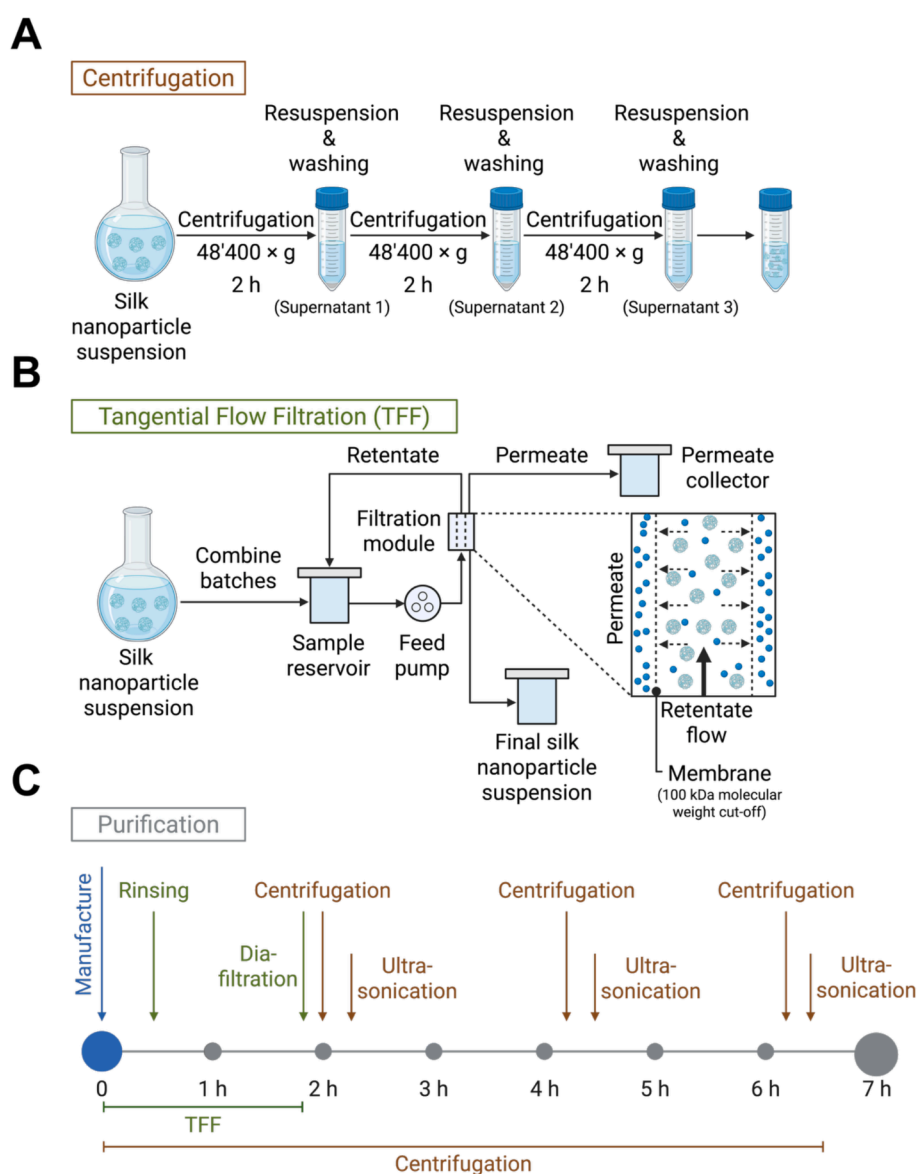


Fig. 1. Schematic overview of the silk nanoparticle purification processes using centrifugation or tangential flow filtration (TFF). (A) For centrifugation, a silk nanoparticle suspension was pelleted (resuspension & washing, supernatant 1); this step was repeated twice, and the silk nanoparticles were resuspended in ultrapure water. (B) For TFF, the silk nanoparticle suspension underwent an initial diafiltration to change isopropanol against ultrapure water. A concentration step then occurred by a final collection of the concentrated silk nanoparticles. All purified silk nanoparticles were stored at 4 °C until use. (C) Timeline summarising the experimental workflows for both purification strategies.

cocoons, as described elsewhere. (Wongpinyochit et al., 2019) Briefly, dried *B. mori* cocoons were cut into approximately 5 × 5 mm pieces and 5 g were degummed with 2 L of 25 mM aqueous Na₂CO₃ at 98–105 °C for 1 h under manual stirring. Degummed silk fibres were rinsed in ultrapure H₂O (1 L) three times for 0.33 h each. The silk was then air-dried for at least 24 h at room temperature. Dry silk fibres were dissolved in a 9.3 M aqueous LiBr solution at 60 °C for 4 h. The silk fibroin solution, denoted as silk solution, was dialysed (MWCO 3,500 Da, Thermo Fisher Scientific Inc., Waltham, MA, USA) against ultrapure H₂O (1 L) for 48 h with six water changes to remove the LiBr salt. The silk solution was then purified by centrifugation over three cycles, each for 0.33 h at 10,000g and 4 °C (Allegra 64 R, Beckman Coulter, California, USA) to remove any aggregates. Silk concentrations were determined gravimetrically and then adjusted to 3 % w/v with ultrapure H₂O (Fig. S1).

Silk Nanoparticle Manufacture in Semi-Batch Format. A semi-batch workflow was used to generate silk nanoparticles, as detailed elsewhere (Fig. S2) (Matthew et al., 2020). Briefly, silk nanoparticles were manufactured at room temperature using a syringe pump (Just Infusion NE-300, New Era Pump Systems, UK) equipped with a 10 mL B. Braun Omnifix® Luer Lock Solo syringe and a blunt needle (23G × 0.25"). The syringe pump inclination was 0–0.1°. The isopropanol antisolvent was added to a 50 mL short-neck round-bottom flask (final 5:1 v/v ratio of isopropanol to silk). Briefly, 6 mL of a freshly prepared 3 % w/v silk solution was added dropwise (1 mL min⁻¹) to 30 mL isopropanol. The silk solution was added from a height of 7.5 cm from the bottom of the isopropanol meniscus and stirred using an oblong stir bar (18 × 6 mm) at 400 rpm. Syringe pump flow rates for the 10 mL B. Braun Omnifix® Luer Solo syringe were calculated based on the manufacturer-specified internal barrel diameter, following the same methodology applied in previous volumetric displacement determinations.

Silk Nanoparticle Purification by Centrifugation. The semi-batch manufactured silk nanoparticles were centrifuged (Allegra 64 R centrifuge equipped with an f1010 fixed-angle aluminium rotor, Beckman Coulter, California, USA) at 48,400 × g for 2 h at 4 °C and the supernatant was aspirated. The pellet was resuspended in ultrapure water (1 mL) and sonicated twice for 30 s at a 30 % amplitude with a Sonopuls HD 200 sonicator equipped with a Sonotrode MS72 sensor (ultrasonic homogeniser, Bandelin, Berlin, Germany). An additional volume of ultrapure water (7 mL) was added, and the centrifugation, washing and resuspension steps were repeated twice. The final pellet was collected and resuspended in 5 mL ultrapure water. This final silk nanoparticle suspension was stored at 4 °C until use.

Silk Nanoparticle Purification by the TFF Method. All experiments were performed using a Cogent® Lab 800 TFF system (MilliporeSigma, Burlington, Vermont, United States) equipped with a Pellicon® 2 cassette consisting of Biomax® polyethersulfone membranes with a nominal molecular weight cut-off of 100 kDa and a total membrane area of 0.1 m² (MilliporeSigma, Burlington, Vermont, United States). The module contained two membranes separated by an A-screen. The cassettes were mounted in a Pellicon® Mini Cassette Holder and torqued to 190 in.-pounds to prevent leakage. The Pellicon® 2 cassettes were flushed with ultrapure water before and after the filtration process. Before every filtration process, the normalised water permeability index was determined at transmembrane pressure (0.5–0.6 bar) and room temperature. Silk nanoparticle suspensions were made as described above, and prior to purification, 5 batches of nanoparticles (approximately 210–360 mg of silk nanoparticles) were combined and added to the TFF system at a final volume of 180 mL. The silk nanoparticle suspensions underwent diafiltration until 68–78 mL of concentrated nanoparticle suspension remained. During the diafiltration process, the transmembrane pressure was maintained at 0.5 bar, the feed pressure was 1 bar, and the feed flow rate was 500 mL min⁻¹. Either 5 or 20 diafiltration volumes were changed until the process was stopped. The final nanoparticle suspension was collected and stored at 4 °C until use.

Yield of Silk Nanoparticles. The production yield was calculated as

detailed previously (Matthew et al., 2020).

Physicochemical Characterisation and Stability Test. The size, PDI and zeta potential of the silk nanoparticles were measured using a Zetasizer Nano ZS dynamic light scattering instrument (Malvern Panalytical GmbH, Malvern, UK). Size and PDI measurements were acquired using three technical replicates per each sample and then averaged for each batch of silk nanoparticles. A single batch, representing a biological replicate, was prepared from a freshly degummed lot of silk fibres. To characterise silk nanoparticle size, 20 µL silk nanoparticle suspension was diluted in 500 µL ultrapure water. Each measurement of size and polydispersity index (PDI) was performed in polystyrene UV cuvettes (Brand GmbH + Co KG, Wertheim, Germany) with 11–13 runs of 30 s after an equilibration time of 120 s, while the backscatter angle was set at 173°. The z-averaged hydrodynamic diameter was calculated using the Stokes–Einstein equation. The data set from 11 to 13 measurements was averaged for each sample. The zeta potential was measured by diluting 50 µL silk nanoparticle suspension in 500 µL ultrapure water. Each zeta potential measurement was implemented in DTS 1070 capillary folding polystyrene cuvettes (Malvern Panalytical GmbH, Malvern, UK). Zeta potentials were calculated based on the Smoluchowski equation. The purified silk nanoparticles were stored in a refrigerator at 4 °C for 37 weeks (TFF samples) and 38 weeks (centrifugation samples). The particle size, PDI and zeta potential were measured again as described elsewhere.

Morphology Analysis. The nanoparticle morphology of all samples was visualised using cryo transmission emission microscopy (Cryo-TEM). A 7 µL volume of each sample was applied to a gold grid covered by a perforated gold film (UltrAuFoil 1.2/1.3 or 2/1, Quantifoil Micro Tools GmbH, Jena, Germany). Excess liquid was automatically blotted, and the samples were rapidly plunge-frozen in liquid ethane (cooled to –180 °C) in a Cryobox (Carl Zeiss NTS GmbH, Oberkochen, Germany). Excess ethane was removed, and the samples were transferred immediately, using a Gatan 626 cryo-transfer holder (Gatan, Pleasanton, USA) mounted into the pre-cooled Cryo-electron microscope (Philips CM 120, Eindhoven, Netherlands) operated at 120 kV and viewed under low-dose conditions. The images were recorded with a 2k CMOS camera (F216, TVIPS, Gauting, Germany). Noise was minimised by recording four images and averaging them to one image.

Secondary Structure of Silk Nanoparticles. Air-dried silk films were used as silk I structure references, while silk films treated for 60 min with 70 % v/v ethanol/ultrapure H₂O were used as positive controls for the silk II structure. Silk films and nanoparticles were analysed by Fourier transform infrared spectroscopy (FTIR) on an ATR-equipped ALPHA II FTIR spectrometer (Bruker Optik GmbH, Ettlingen, Germany). Each silk nanoparticle sample was flash-frozen at –80 °C for 5 h prior to lyophilisation at –30 °C and 0.140 mbar for 24 h following a post-drying phase at 0 °C for 17 h. Each FTIR measurement was run for 128 scans at a 4 cm⁻¹ resolution in absorption mode over the wavenumber range of 400–4000 cm⁻¹ and corrected for atmospheric absorption using Opus software (Bruker Optik GmbH, Ettlingen, Germany). The amide I regions of the FTIR spectra were analysed in OriginLab 2024 (Northampton, MA, USA), as described elsewhere. (Yang et al., 2015) The second derivative of the background-corrected absorption spectrum was obtained and smoothed twice using a seven-point Savitzky-Golay function with a polynomial order of 2. A nonzero baseline was interpolated between 2 and 3 of the highest points between 1600 and 1710 cm⁻¹. Peak positions in the amide I region were then identified using the second derivative and peaks fitted using nonlinear least squares with a series of Gaussian curves. Band positions, widths and heights were allowed to vary, and the peak area was allowed to take any value below or equal to 0. The deconvoluted spectra were area-normalised, and the secondary structure content was calculated with reference to literature band assignments (Asakura, 2021; Hu et al., 2006; Shimanovich et al., 2017) using the relative areas of each band. The correlation coefficient was calculated as described elsewhere. (Matthew et al., 2020) The air-dried silk film of an aqueous silk precursor batch

was used as the reference for all silk films and silk nanoparticle samples. The silk sample and reference were compared between 1600 and 1700 cm^{-1} according to equation (1):

$$R = \left(\frac{\sum x_i y_i}{\sqrt{\sum x_i^2 \sum y_i^2}} \right) \quad (1)$$

where x_i and y_i are the derivative values of the reference and silk sample at the frequency i .

3. Isopropanol quantification of silk nanoparticles

Isopropanol concentrations were determined using a Clarus 500 gas chromatograph equipped with a Perkin-Elmer TurboMatrix 40 headspace sampler (Perkin-Elmer, Shelton, CT USA). Samples were diluted with H_2O and spiked with the internal standard *tert*-butyl alcohol (5×10^{-3} % v/v). A splitless headspace injection was performed applying the following conditions: sample temperature 60 °C, needle temperature 70 °C, transfer line temperature 110 °C, thermostating time 20 min, pressurisation time 2 min, injection time 0.04 min, dwell time 0.1 min and a column pressure of 90 kPa. Analyte separation was performed with an Elite-BAC1 Advantage Capillary Column (30 m, 0.53 mm, 3.00 μm film thickness; Perkin-Elmer) with isothermal chromatographic separation at 35 °C and nitrogen as the carrier gas (3 mL min^{-1}). The flame ionisation detector temperature was 250 °C and detector gases were air (400 mL min^{-1}) and hydrogen (45 mL min^{-1}). Isopropanol concentrations were calculated using an aqueous six-point calibration curve (31–1000 mg L^{-1}). Data acquisition and integration were carried out using TotalChrom software (version 6.3.2.0646).

4. In vitro cytotoxicity of silk nanoparticles

Murine J774A.1 macrophages were purchased from Cytion (Cytion, Eppelheim, Germany). The cells were cultured in Dulbecco's Modified Eagle Medium (DMEM; containing 4.5 g glucose, sodium pyruvate, L-glutamine and phenol red) (Gibco, Paisley, UK) supplemented with 10 % v/v foetal bovine serum (FBS) (Gibco, Paisley, UK) and maintained in a humidified 5 % CO_2 atmosphere at 37 °C. The cells were routinely subcultured at 70–90 % confluency by aspirating the medium, washing twice with phosphate buffered saline (PBS) and incubating with TrypLE™ Express (Gibco, Grand Island, NY). Complete medium was then added, and the cell suspension was centrifuged for 5 min at $200 \times g$. The cell pellet was then resuspended in DMEM with 10 % FBS and the cells were replated in flat-bottom 96-well polystyrene plates (Greiner bio. one, Frickenhausen, Germany) at a density of 1×10^4 cells/ cm^2 and allowed to recover for 24 h at 37 °C, 5 % CO_2 . Then, 10 μL of silk nanoparticles, purified either through centrifugation or tangential flow filtration, were added at concentrations of 1–500 $\mu\text{g mL}^{-1}$ (as aqueous suspensions) to the medium and incubated for 48 h at 37 °C, and 5 % CO_2 . H_2O -treated cells served as controls. Cell metabolic activity was assessed by adding 11 μL of 3-(4,5-dimethylthiazol-2-yl)-2,5-diphenyltetrazoliumbromide (MTT, final concentration of 0.5 mg mL^{-1} in PBS) to each well and incubating for 2 h. The supernatant was aspirated and 100 μL DMSO (BioScience Grade, Roth, Karlsruhe, Germany) was added to each well. The absorbance was measured at wavelength $\lambda = 570 \text{ nm}$ with background correction at $\lambda = 630 \text{ nm}$ using a Tecan Spark multimode plate reader (Tecan Spark 20 M, Tecan, Männedorf, Switzerland). Relative metabolic activity was calculated as a percentage by normalising to H_2O -treated cells.

The human A549 adenocarcinomic alveolar basal epithelial cell line (Leibniz Institute DSMZ, German Collection of Microorganisms and Cell Cultures GmbH, Braunschweig, Germany) was cultured in an incubator (37 °C; 5 % CO_2 ; relative humidity of 95 %) in DMEM (Gibco) low glucose (1 g/L) cell culture medium, supplemented with 10 % v/v foetal bovine serum (FBS, Gibco) and 4 mM of stable L-alanyl-glutamine (GlutaMAX™) (all purchased from ThermoFisher Scientific, Darmstadt, Germany). At a confluency of approx. 80–90 %, the cells were passaged

at split ratios of 1:5 to 1:10, usually every two to three days. For this, cells were washed with PBS, detached with TrypLE™ Express Enzyme (Gibco, Grand Island, NY), and complete medium was added before centrifugation for 5 min at $200 \times g$. Cells were resuspended in complete medium, seeded into flat-bottom 96-well polystyrene plates (Greiner bio. one, Frickenhausen, Germany) at a cell density of 5×10^4 cells mL^{-1} and grown under controlled conditions (37 °C; 5 % CO_2 ; relative humidity of 95 %). After 24 h, the medium was refreshed, and a 10 μL of sample (i.e., aqueous silk nanoparticle suspensions at different concentrations, ranging from 1 to 500 $\mu\text{g mL}^{-1}$) was added per well. Cells treated with H_2O only served as controls. Treated cells were incubated for a further 48 h under standard cell culture conditions (37 °C; 5 % CO_2 ; relative humidity of 95 %) prior to subsequent analysis. Cell metabolic activity was assessed by adding 11 μL of MTT to each well to reach a final concentration of 0.5 mg mL^{-1} . After incubation at 37 °C for 3 h samples were prepared and measured as detailed above.

Statistical Analyses and Data Presentation. Data were compiled using Microsoft® Excel® version 16.94 (Microsoft Office 365 ProPlus for Mac, Redmond, WA, USA). FTIR data were processed using OriginPro version 2024 (OriginLab Corporation, Northampton, MA, USA). Graphs and statistical analyses were prepared using GraphPad Prism 10.4.1 (GraphPad Software, Boston, MA, USA). Statistical tests include one-way analysis of variance, followed by Dunnett's post hoc test, was conducted for comparisons between multiple groups. Sample pairs were analysed by either a paired or unpaired *t*-test. Normality and homogeneity of variances were assumed. Asterisks denote statistical significance as follows: $p < 0.05$ (*), $p < 0.01$ (**), and $p < 0.001$ (***). All data are presented as mean values \pm standard deviation, and the number of independent experiments (n) is provided in each figure legend.

5. Results

Nanoparticle Morphology, Size, and Surface Charge. The silk nanoparticle morphology was analysed using Cryo-TEM. All particles prepared from degummed silk had a spherical shape (Fig. 2a).

Standard centrifugation purified silk nanoparticles showed the most uniform morphology. These results correlated well with the polydispersity indices obtained by dynamic light scattering measurements (Fig. 2b). The use of TFF for purification retained regularly shaped particles, but with wider size distributions, as quantified using dynamic light scattering (Fig. S4). The largest nanoparticles (95 nm) were obtained using 20 diavolumes during TFF. Polydispersity was higher for TFF purification (PDI of 0.181–0.235) compared to purification using centrifugation (polydispersity index 0.108), (Fig. 2b). However, comparison of nanoparticles prepared by centrifugation and TFF, showed no substantial differences in size or polydispersity, whereas the surface charge decreased from -39 mV to less negative values of -23 mV for 5 diavolumes changed by TFF. A 20 diavolume change using TFF resulted in an increase in negative values up to -53 mV (Fig. 2b). The stability of the silk nanoparticles was explored in ultrapure water at 4 °C after 37 and 38 weeks of storage in the refrigerator. The consistency in size, PDI and zeta potential over time shows stable formulations for centrifugation and TFF purified silk nanoparticles (Fig. 2b). Overall, the yields ranged from approximately 8 % for centrifugation to 25 % for TFF. The higher yields with TFF were a result of less losses when compared to centrifugation resulting in the collection of more particles during sample purification. For TFF five batches were combined to reach the minimum volume for a run of the system.

Analysis of the Secondary Structure of Silk Films and Nanoparticles. The impact of the purification process on the secondary structure of silk nanoparticle was determined by attenuated total reflectance-FTIR (ATR-FTIR) analysis and deconvolution of the characteristic protein amide I band ($1600\text{--}1710 \text{ cm}^{-1}$) (Fig. S5). The secondary structure did not vary significantly whether the particles were purified by centrifugation or TFF.

For centrifugation and TFF purification, the β -sheet content (62–66

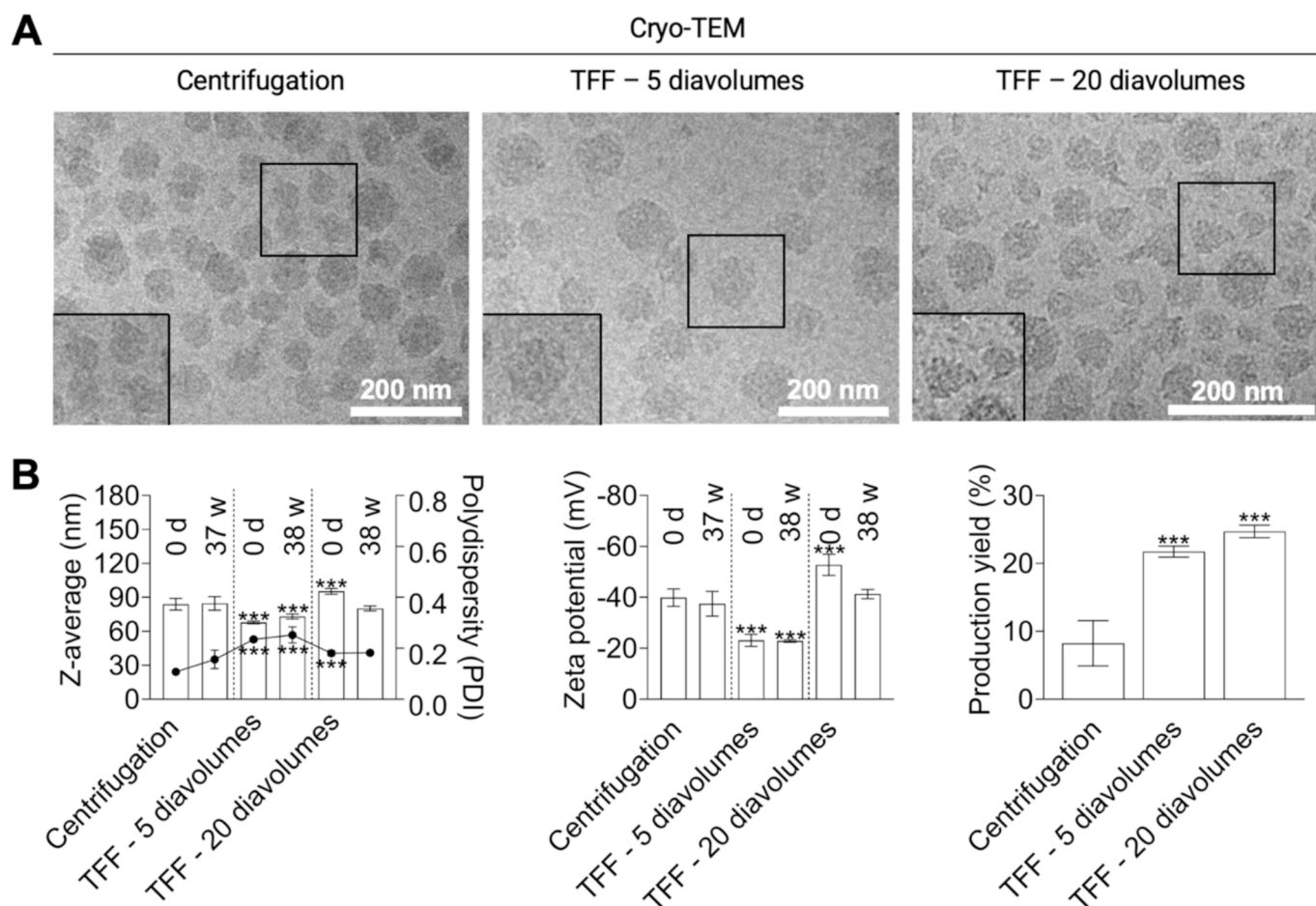


Fig. 2. Physicochemical characteristics of silk nanoparticles in response to purification by centrifugation versus tangential flow filtration (TFF). (A) Cryo transmission electron microscopy (Cryo-TEM) images of silk nanoparticles manufactured in semi-batch format ($n = 1$). (B) Analysis of size (dynamic light scattering, DLS; polydispersity index, PDI), zeta potential (ZP) (electrophoretic light scattering, ELS), and production yield of silk nanoparticles ($n = 3$ for centrifugation and $n = 5$ for TFF). Size, polydispersity and zeta potential were measured after 0 days (d) and 37 weeks (w) (centrifugation) or 38 weeks (w) (TFF). Error bars are hidden in the bars and plot symbols when not visible, mean \pm SD. Multiple groups were evaluated by one way analysis of variance (ANOVA), followed by Dunnett's multiple comparison post hoc test (controls are centrifugation samples). Asterisks denote statistical significance determined using post hoc tests as follows: $p < 0.05$ (*), $p < 0.01$ (**), and $p < 0.001$ (***)

%) was higher than for ethanol-treated silk films (59 %), which served as a positive control for the silk II structure (Fig. 3). Additionally, the random coil contents (10–13 %) of the silk nanoparticles were comparable to those of the ethanol-treated films (18 %). The silk nanoparticles purified by centrifugation or TFF showed a significantly higher percentage of β -sheets and lower random coil content compared to the negative silk II structure control (air-dried silk film with 44 % β -sheet and 36 % random coil content). A correlation coefficient method was used to compare the second-derivative ATR-FTIR spectra in the amide I region (1600–1700 cm^{-1}) to measure formulation-induced structural changes in silk nanoparticles versus those in an air-dried silk film. The silk nanoparticle correlation coefficients for both purification methods ranged from 0.21 to 0.27.

In Vitro Cytotoxicity of Silk Nanoparticles. The biocompatibility of silk nanoparticles was tested using murine J774A.1 macrophage cells and human A549 lung adenocarcinoma cells. The silk nanoparticles purified by centrifugation exhibited the lowest cytotoxicity in both cell lines. These samples had the lowest residual isopropanol content ($57.5 \pm 0.7 \text{ mg L}^{-1}$) when compared to TFF samples (ranging from $103.5 - 2215 \text{ mg L}^{-1}$, detailed below). Nanoparticles prepared using TFF purification with a change of only 5 diavolumes had the highest cytotoxicity and those prepared using 20 diavolumes were still more cytotoxic than the centrifugation-purified nanoparticles. Quantification of residual isopropanol of 5 and 20 diavolume samples were $103.5 \pm 2.12 \text{ mg L}^{-1}$

and $2215.0 \pm 35.5 \text{ mg L}^{-1}$, respectively. The cytotoxicity of all tested nanoparticles was lower for the A549 cells than for the J774A.1 cells. Cell viability gradually decreased over the tested concentration range from low to high. The IC_{50} was greater than $500 \mu\text{g mL}^{-1}$ (Fig. 4) for the centrifugation-purified nanoparticles in both cell lines and for the TFF-purified nanoparticles (20 diavolumes) in the A549 cells.

6. Discussion

Silk has emerged as a promising biopolymer for drug and gene delivery applications across different material formats, including particles. (Pollini & Paladini, 2024; Tomeh et al., 2019) A wide range of fabrication techniques has been reported, yielding silk-based particles ranging in size from the nano- to the microscale. (Matthew & Seib, 2025) However, these manufacturing processes are sensitive to numerous parameters that affect the physicochemical properties of the final product. (Kumari et al., 2023) This complexity poses significant challenges when attempting to boost production from the laboratory to the industrial scale. (Bari, 2020; Matthew et al., 2022) Recent advances in microfluidics help to overcome scale-up and reproducibility challenges by enabling precise control of reaction parameters and continuous processing for producing suitable drug delivery systems. (Wongpinyochit et al., 2019; Mansor et al., 2025; Zhang et al., 2025) However, advanced purification methods of protein-based nanocarriers are often lagging

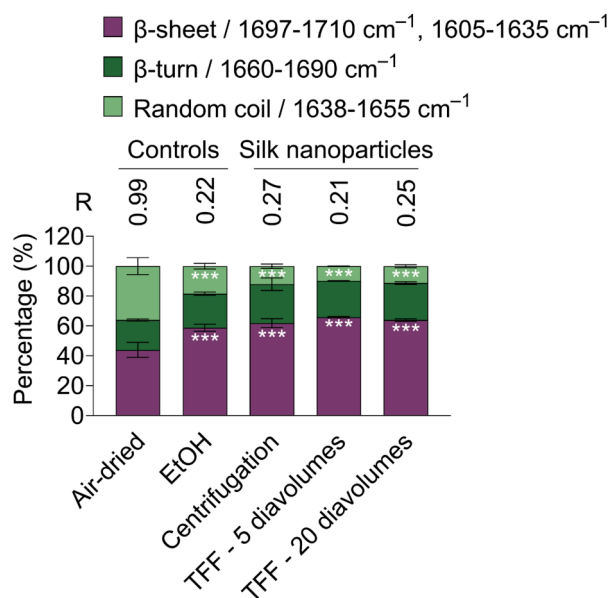


Fig. 3. Secondary structure determination of silk nanoparticles. Silk nanoparticles manufactured in semi-batch format and purified using centrifugation or TFF. The relative area of the assigned peaks in the second derivative spectrum was used to calculate the secondary structure content (%). The positive silk II control was defined as the 70 % v/v ethanol/ultrapure H₂O annealed sample. The negative silk II control was defined as the air-dried silk film and was defined as the reference for the spectral correlation coefficients of all sample types. Statistical analyses: Two-way ANOVA and Dunnett's multiple comparisons test (control air-dried sample) for secondary structure content; $p < 0.05$ (*), $p < 0.01$ (**), and $p < 0.001$ (***). Abbreviations: ANOVA: analysis of variance; EtOH: ethanol; TFF: tangential flow filtration.

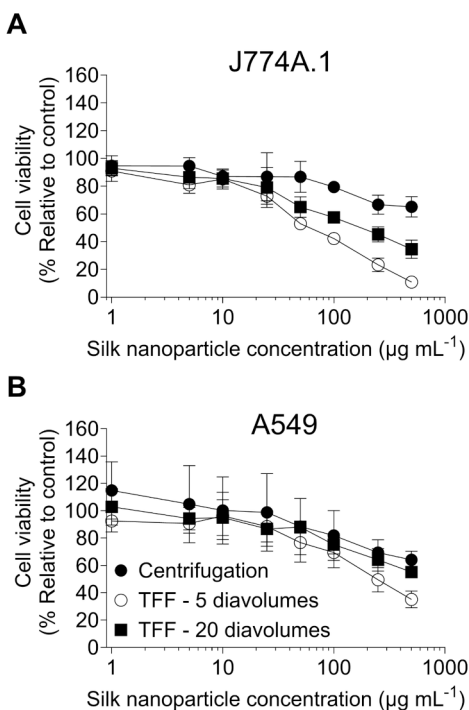


Fig. 4. Impact of purification method on silk nanoparticle cytotoxicity. In vitro cytotoxicity in different cell lines (J774A.1 and A549) in response to treatment for 48 h with centrifugation-purified and TFF-purified silk nanoparticles at different concentrations, ranging from 1 to 500 $\mu\text{g mL}^{-1}$. Error bars are hidden in the plot-symbol when not visible, mean \pm SD, (J774A.1: $n = 3$; A549: $n = 6$ biological repeats).

behind these developments. (Agrawal et al., 2023).

Many conventional fabrication techniques involve the use of organic solvents or give rise to residual impurities that may compromise the safety and efficacy of the nanoparticles. Centrifugation is the most commonly employed purification method; however, it is constrained by batch size, scalability and prolonged processing times. To address these limitations, this study compared the effects of centrifugation and tangential flow filtration (TFF) on the critical quality attributes of silk nanoparticles, namely morphology, size, polydispersity, zeta potential, yield and secondary structure. Centrifugation served as the reference purification method, while TFF was evaluated under constant flow rate (500 mL min^{-1}) and transmembrane pressure (0.5 bar). Two diafiltration volumes—5 and 20 diavolumes—were tested to assess the impact of solvent exchange on nanoparticle characteristics. Significant differences were observed between the two purification methods (Fig. 2b). Centrifugation resulted in a notable yield loss, likely due to the removal of smaller nanoparticles retained in the supernatant. In contrast, the permeate from TFF was clear, indicating minimal nanoparticle loss. The minor yield reductions in TFF are presumed to arise from residual volume in the tubing and possible membrane fouling. Maintaining a high flow rate and low transmembrane pressure was essential to minimise shear stress and from membrane fouling and to preserve particle morphology.

Both purification methods produced spherical nanoparticles (Fig. 2a). However, the particle size varied depending on the method and diafiltration volume. TFF with 20 diavolumes yielded the largest nanoparticles (95.4 nm), slightly larger than those from centrifugation (84 nm). The smallest nanoparticles (67.9 nm) were observed with TFF at 5 diavolumes. Regarding polydispersity, the centrifugation-purified nanoparticles were the most monodisperse nanoparticles (0.108), followed by TFF with 20 diavolumes (0.181), and the least uniform particles were obtained with TFF at 5 diavolumes (0.235). We hypothesise that the higher polydispersity value resulted from minimal nanoparticle loss during purification, which preserved a more heterogeneous particle population. In addition, the absence of centrifugation-induced fractionation further contributed to the broader size distribution. Residual isopropanol could further impact particle attributes too; the raised organic fraction in immediate nanoparticle proximity could impact solvent-silk interactions giving rise to a wider size distribution. (Bovone et al., 2022) TFF generally enables gentler sample handling but has limited sample fractionation potential. (Özçelik & Zeynep Çulfaz-Emecen, 2025; Shah et al., 2020) TFF systems are widely used in the pharmaceutical industry for product clean-up. Our system was operated according to the manufacturer's standard operating procedure. The system was thoroughly washed, exceeding the dead volume severalfold. Therefore, the risk that extractables contaminated the final product can be regarded as very low (Menzel et al., 2023).

The zeta potential measurements further highlighted the influence of purification on surface charge, with TFF with 20 diavolumes producing the most negatively charged particles (-53 mV), followed by centrifugation (-40 mV) and TFF with 5 diavolumes (-23 mV). These findings suggest that the purification efficiency significantly impacts the electrokinetic stability of silk nanoparticles. The silk nanoparticles from both purification methods showed a high long-term stability (Fig. 2b). Secondary structure analysis (Fig. 3) revealed minor differences, particularly in the TFF sample with 5 diavolumes. Isopropanol acts as a crystallising agent, enhancing β -sheet content, which is desirable for silk nanoparticle physical stability. (Kaewpirom & Boonsang, 2020) However, inadequate solvent removal is problematic from a clinical perspective and may therefore lead to limited pharmaceutical utility.

The biocompatibility of the silk nanoparticles was assessed using murine J774A.1 macrophage cells and human A549 lung adenocarcinoma cells across a concentration range of $1\text{--}500 \mu\text{g mL}^{-1}$. Both cell lines exhibited a similar trend: nanoparticles purified via centrifugation induced the lowest cytotoxicity, followed by TFF with 20 diavolumes. The highest cytotoxic effects were observed with the less purified TFF

samples (5 diavolumes). Notably, A549 cells were generally more tolerant than J774A.1 cells, likely reflecting inherent differences in cell line sensitivity towards nanoparticles as reported previously. (Lu et al., 2014; Tietze et al., 2025) These findings underscore the critical role of purification in defining the safety profile of silk-based nanocarriers.

Looking ahead, several key areas merit further investigation. Process modelling and design-of-experiment (DoE) approaches could be employed for systematic optimisation of the TFF parameters (e.g., diafiltration volume, membrane cut-off, transmembrane pressure and shear rate) to balance throughput, product quality and cost-efficiency. (Shah et al., 2020) Comparative analyses of different purification strategies—including chromatography or hybrid approaches—could reveal alternative or complementary methods for producing high-purity silk nanoparticles suitable for biomedical applications. Furthermore, TFF is well suited to purify and subsequently characterise key quality attributes of drug-loaded silk nanoparticles, including encapsulation efficiency, drug-loading capacity and in vitro release.

7. Conclusions

Progressing the production of silk nanoparticles from bench to market requires insight into the impact of the purification process on the physicochemical properties of the final nanoparticle product. In this study, we used TFF for silk nanoparticle purification and compared it to centrifugation. We found that the critical nanoparticle quality attributes are not substantially affected by the choice of purification method. However, the yield at the end of the two purification methods was substantially higher when using TFF for purification. Further advantages include scalability and time saving when using TFF. However, TFF was less efficient at solvent clearance under the tested conditions. This limitation was reflected in the higher residual isopropanol levels. One key parameter influencing solvent removal in TFF was the change in volume during diafiltration; this factor, requires further optimisation of system-related parameters, such as transmembrane pressure and flow rate, to enhance purification efficiency. Overall, the study findings showed the potential of TFF as alternative purification method but also underscore the need for systematic process development to improve TFF performance, particularly in terms of solvent exchange, to establish it as a robust and scalable purification strategy for silk nanoparticles suitable for biomedical applications.

CRedit authorship contribution statement

Manuel Fischer: Writing – original draft, Visualization, Methodology, Investigation, Formal analysis, Data curation. **Annika Kahlenberg:** Writing – review & editing, Methodology, Investigation, Formal analysis, Data curation. **Simone Berger:** Writing – review & editing, Methodology, Investigation, Formal analysis, Data curation. **Frank Steiniger:** Methodology, Investigation, Formal analysis, Data curation. **Daniela Wissenbach:** Writing – review & editing, Methodology, Investigation, Formal analysis, Data curation. **F. Philipp Seib:** Writing – review & editing, Supervision, Resources, Project administration, Methodology, Funding acquisition, Formal analysis, Conceptualization.

Declaration of competing interest

The authors declare that they have no known competing financial interests or personal relationships that could have appeared to influence the work reported in this paper.

Acknowledgements

The authors would like to thank Dr. Jana Thamm for their helpful discussion. F.P.S. acknowledges support from a DFG Heisenberg grant (SE 3307/1-1) and funding from the Free State of Thuringia (Thüringer Aufbaubank) and European Fonds for Regional Development (EFRE)

with grant no. 2024FGI0005. This work was supported by the Fraunhofer Internal Programs under Grant No. Attract 40-04900. F.P.S. holds the endowed CZS Professorship for Pharmaceutical Technology and Biopharmaceutics funded by the Carl-Zeiss-Stiftung.

Appendix A. Supplementary material

Supplementary data to this article can be found online at <https://doi.org/10.1016/j.ijpharm.2025.126436>.

Data availability

All data created during this research are openly available from: <https://doi.org/10.5281/zenodo.17806063>.

References

- Agrawal, P., Wilkstein, K., Guinn, E., Mason, M., Serrano Martinez, C.I., Saylae, J., 2023. A review of tangential flow filtration: process development and applications in the pharmaceutical industry. *Org. Process Res. Dev.* 27 (4), 571–591. <https://doi.org/10.1021/acs.oprd.2c00291>.
- Asakura, T., 2021. Structure of silk I (Bombyx mori silk fibroin before spinning) -type II β -turn. *Not α -Helix*. *Molecules* 26 (12), 3706. <https://doi.org/10.3390/molecules26123706>.
- Baimark, Y., Srihanam, P., Srisuwan, Y., Phinyocheep, P., 2010. Preparation of porous silk fibroin microparticles by a water-in-oil emulsification-diffusion method. *J. Appl. Polym. Sci.* 118 (2), 1127–1133. <https://doi.org/10.1002/app.32506>.
- Bari, E., 2020. From bench to bedside: the long way towards GMP scale-up, preclinical and clinical trials for silk-based drug delivery systems. In: Bari, E., Perteghella, S., Torre, M.L. (Eds.), *Silk-based Drug Delivery Systems* (pp. 179–204). The Royal Society of Chemistry. <https://doi.org/10.1039/9781839162664-00179>.
- Bovone, G., Cousin, L., Steiner, F., Tibbitt, M.W., 2022. Solvent controls nanoparticle size during nanoprecipitation by limiting block copolymer assembly. *Macromolecules* 55 (18), 8040–8048. <https://doi.org/10.1021/acs.macromol.2c00907>.
- Dalwadi, G., Benson, H.A.E., Chen, Y., 2005. Comparison of diafiltration and tangential flow filtration for purification of nanoparticle suspensions. *Pharm. Res.* 22 (12), 2152–2162. <https://doi.org/10.1007/s11095-005-7781-z>.
- Dalwadi, G., Sunderland, B., 2008. Comparison and validation of drug loading parameters of PEGylated nanoparticles purified by a diafiltration centrifugal device and tangential flow filtration. *Drug Dev. Ind. Pharm.* 34 (12), 1331–1342. <https://doi.org/10.1080/03639040802098177>.
- Dalwadi, G., Sunderland, V.B., 2007. Purification of PEGylated nanoparticles using tangential flow filtration (TFF). *Drug Dev. Ind. Pharm.* 33 (9), 1030–1039. <https://doi.org/10.1080/03639040601180143>.
- Dizon-Maspat, J., Bourret, J., D'Agostini, A., Li, F., 2012. Single pass tangential flow filtration to debottleneck downstream processing for therapeutic antibody production. *Biotechnol. Bioeng.* 109 (4), 962–970. <https://doi.org/10.1002/bit.24377>.
- Gagnon, P., 2012. Technology trends in antibody purification. *J. Chromatogr. A* 1221, 57–70. <https://doi.org/10.1016/j.chroma.2011.10.034>.
- Holland, C., Numata, K., Rnjak-Kovacina, J., Seib, F.P., 2019. The biomedical use of Silk: past, present, future. *Adv. Healthcare Mater.* 8 (1), 1800465. <https://doi.org/10.1002/adhm.201800465>.
- Hu, X., Kaplan, D., Cebe, P., 2006. Determining beta-sheet crystallinity in fibrous proteins by thermal analysis and infrared spectroscopy. *Macromolecules* 39 (18), 6161–6170. <https://doi.org/10.1021/ma0610109>.
- Kaewpirom, S., Boonsang, S., 2020. Influence of alcohol treatments on properties of silk-fibroin-based films for highly optically transparent coating applications. *RSC Adv.* 10 (27), 15913–15923. <https://doi.org/10.1039/D0RA02634D>.
- Kumari, S., Raturi, S., Kulshrestha, S., Chauhan, K., Dhingra, S., András, K., Thu, K., Khargotra, R., Singh, T., 2023. A comprehensive review on various techniques used for synthesizing nanoparticles. *J. Mater. Res. Technol.* 27, 1739–1763. <https://doi.org/10.1016/j.jmrt.2023.09.291>.
- Liu, Y., Yang, G., Jin, S., Xu, L., Zhao, C., 2020. Development of high-drug-loading nanoparticles. *ChemPlusChem* 85 (9), 2143–2157. <https://doi.org/10.1002/cplu.202000496>.
- Lu, Y., Su, S., Jin, W., Wang, B., Li, N., Shen, H., Li, W., Huang, Y., Chen, H., Zhang, Y., Chen, Y., Lin, N., Wang, X., Tao, S., 2014. Characteristics and cellular effects of ambient particulate matter from Beijing. *Environ. Pollut.* 191, 63–69. <https://doi.org/10.1016/j.envpol.2014.04.008>.
- Mansor, M.H., Gao, Z., Howard, F., MacInnes, J., Zhao, X., Muthana, M., 2025. Efficient and rapid microfluidics production of bio-inspired nanoparticles derived from Bombyx mori silkworm for enhanced breast cancer treatment. *Pharmaceutics* 17 (1), 95. <https://doi.org/10.3390/pharmaceutics17010095>.
- Matthew, S.A.L., Rezwani, R., Perrie, Y., Seib, F.P., 2022. Volumetric scalability of microfluidic and semi-batch silk nanoprecipitation methods. *Molecules* 27 (7), 2368. <https://doi.org/10.3390/molecules27072368>.
- Matthew, S.A.L., Seib, F.P., 2025. The dawning era of anticancer nanomedicines: from first principles to application of silk nanoparticles. *Advanced Therapeutics* 8 (1), 2400130. <https://doi.org/10.1002/adtp.202400130>.

- Matthew, S.A.L., Totten, J.D., Phuagkhaopong, S., Egan, G., Witte, K., Perrie, Y., Seib, F. P., 2020. Silk nanoparticle manufacture in semi-batch format. *ACS Biomater Sci. Eng.* 6 (12), 6748–6759. <https://doi.org/10.1021/acsbomaterials.0c01028>.
- Menzel, R., Pahl, I., Loewe, T., Stuetzer, A., Hauk, A., 2022. Rinsing recommendations for membrane filters and identification of rinsables. *Eur. J. Pharm. Sci.* 168, 105982. <https://doi.org/10.1016/j.ejps.2021.105982>.
- Mihaila, R., Chang, S., Wei, A.T., Hu, Z.Y., Ruhela, D., Shadel, T.R., Duenwald, S., Payson, E., Cunningham, J.J., Kuklin, N., Mathre, D.J., 2011. Lipid nanoparticle purification by spin centrifugation–dialysis (SCD): a facile and high-throughput approach for small scale preparation of siRNA–lipid complexes. *Int. J. Pharm.* 420 (1), 118–121. <https://doi.org/10.1016/j.ijpharm.2011.08.017>.
- Mülhopt, S., Diabaté, S., Dilger, M., Adelhelm, C., Anderlohr, C., Bergfeldt, T., Gómez De La Torre, J., Jiang, Y., Valsami-Jones, E., Langevin, D., Lynch, I., Mahon, E., Nelissen, I., Piella, J., Puentes, V., Ray, S., Schneider, R., Wilkins, T., Weiss, C., Paur, H.-R., 2018. Characterization of nanoparticle batch-to-batch variability. *Nanomaterials* 8 (5), 311. <https://doi.org/10.3390/nano8050311>.
- Musumeci, T., Leonardi, A., Bonaccorso, A., Pignatello, R., Puglisi, G., 2018. Tangential flow filtration technique: an overview on nanomedicine applications. *Pharm. Nanotechnol.* 6 (1), 48–60. <https://doi.org/10.2174/2211738506666180306160921>.
- Özçelik, F., Zeynep Çulfaz-Emecan, P., 2025. Nanoparticle concentration and solvent exchange via organic solvent ultrafiltration. *Sep. Purif. Technol.* 354, 129052. <https://doi.org/10.1016/j.seppur.2024.129052>.
- Pollini, M., Paladini, F., 2024. The emerging role of silk fibroin for the development of novel drug delivery systems. *Biomimetics* 9 (5), 295. <https://doi.org/10.3390/biomimetics9050295>.
- Shah, N.K., Ivone, R., Shen, J., Meenach, S.A., 2020. A comparison of centrifugation and tangential flow filtration for nanoparticle purification: a case study on acetalated dextran nanoparticles. *Particuology* 50, 189–196. <https://doi.org/10.1016/j.partic.2019.06.004>.
- Shimanovich, U., Ruggeri, F.S., De Genst, E., Adamcik, J., Barros, T.P., Porter, D., Müller, T., Mezzenga, R., Dobson, C.M., Vollrath, F., Holland, C., Knowles, T.P.J., 2017. Silk micrococoon for protein stabilisation and molecular encapsulation. *Nat. Commun.* 8 (1), 15902. <https://doi.org/10.1038/ncomms15902>.
- Taha, M.S., Padmakumar, S., Singh, A., Amiji, M.M., 2020. Critical quality attributes in the development of therapeutic nanomedicines toward clinical translation. *Drug Deliv. Transl. Res.* 10 (3), 766–790. <https://doi.org/10.1007/s13346-020-00744-1>.
- Tehrani, S.F., Garcia Ac, A., Minani Tuyaga, M.A., Rode Garcia, T., Banquy, X., Roullin, V.G., 2025. Critical assessment of purification processes for the robust production of polymeric nanomedicine. *Int. J. Pharm.* 668, 124975. <https://doi.org/10.1016/j.ijpharm.2024.124975>.
- Tietze, L., Urbano, L., Eisenmann, S., Schwarzingler, J., Kollan, J., Forbes, B., Dailey, L.A., Hädrich, G., 2025. High content image analysis of cellular responses of the murine J774A.1 cell line and primary human cells alveolar macrophages to an extended panel of pharmaceutical agents. *Pharm. Res.* 42 (1), 93–108. <https://doi.org/10.1007/s11095-024-03806-y>.
- Tomeh, M.A., Hadianamrei, R., Zhao, X., 2019. Silk fibroin as a functional biomaterial for drug and gene delivery. *Pharmaceutics* 11 (10), 494. <https://doi.org/10.3390/pharmaceutics11100494>.
- Tomeh, M.A., Mansor, M.H., Hadianamrei, R., Sun, W., Zhao, X., 2022. Optimization of large-scale manufacturing of biopolymeric and lipid nanoparticles using microfluidic swirl mixers. *Int. J. Pharm.* 620, 121762. <https://doi.org/10.1016/j.ijpharm.2022.121762>.
- Tran, H.A., Hoang, T.T., Maraldo, A., Do, T.N., Kaplan, D.L., Lim, K.S., Rnjak-Kovacina, J., 2023. Emerging silk fibroin materials and their applications: new functionality arising from innovations in silk crosslinking. *Mater. Today* 65, 244–259. <https://doi.org/10.1016/j.mattod.2023.03.027>.
- Wongpinyochit, T., Totten, J.D., Johnston, B.F., Seib, F.P., 2019. Microfluidic-assisted silk nanoparticle tuning. *Nanoscale Adv.* 1, 873–883. <https://doi.org/10.1039/C8NA00208H>.
- Xu, M., Qi, Y., Liu, G., Song, Y., Jiang, X., Du, B., 2023. Size-dependent *in vivo* transport of nanoparticles: implications for delivery, targeting, and clearance. *ACS Nano* 17 (21), 20825–20849. <https://doi.org/10.1021/acsnano.3c05853>.
- Zhang, B., Deng, Y., Xu, D., Zhao, X., 2025. Dimethylcurcumin and copper sulfate-loaded silk nanoparticles for synergistic therapy against breast cancer. *ACS Biomater Sci. Eng.* 11 (3), 1539–1548. <https://doi.org/10.1021/acsbomaterials.4c02389>.